

# PCCP

Accepted Manuscript



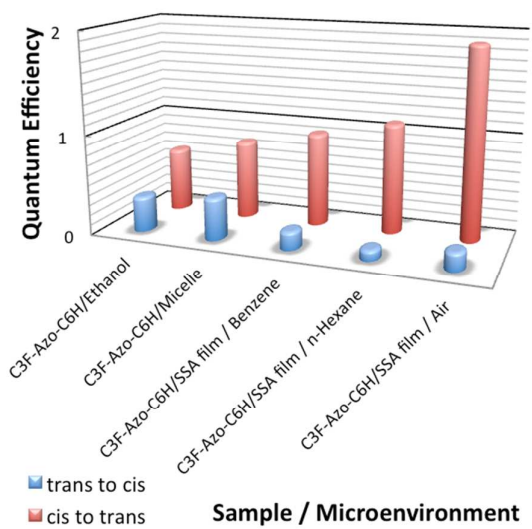
This is an *Accepted Manuscript*, which has been through the Royal Society of Chemistry peer review process and has been accepted for publication.

*Accepted Manuscripts* are published online shortly after acceptance, before technical editing, formatting and proof reading. Using this free service, authors can make their results available to the community, in citable form, before we publish the edited article. We will replace this *Accepted Manuscript* with the edited and formatted *Advance Article* as soon as it is available.

You can find more information about *Accepted Manuscripts* in the [Information for Authors](#).

Please note that technical editing may introduce minor changes to the text and/or graphics, which may alter content. The journal's standard [Terms & Conditions](#) and the [Ethical guidelines](#) still apply. In no event shall the Royal Society of Chemistry be held responsible for any errors or omissions in this *Accepted Manuscript* or any consequences arising from the use of any information it contains.

## Graphical abstract



The quantum yield of photo-isomerization exceeds unity ( $\Phi = 1.9$ ) in organic/inorganic nano-layered microenvironment,

# Remarkable enhancement of the photoreactivity of polyfluoroalkyl azobenzene derivative in organic/inorganic nano-layered microenvironment

Cite this: DOI: 10.1039/x0xx00000x

Received  
Accepted

DOI: 10.1039/x0xx00000x

[www.rsc.org/](http://www.rsc.org/)

Vivek Ramakrishnan,<sup>a</sup> Daisuke Yamamoto,<sup>a,b</sup> Shin Sasamoto,<sup>a</sup> Tetsuya Shimada,<sup>a,b</sup> Yu Nabetani,<sup>a,b</sup> Hiroshi Tachibana,<sup>a,b</sup> and Haruo Inoue<sup>a,b\*</sup>

Organic/inorganic hybrids composed of polyfluoroalkyl azobenzene surfactant (abbreviated as C3F-Azo-C6H) and inorganic layered compounds are able to show reversible three-dimensional morphology changes such as interlayer space change and nanosheet sliding in a giant scale due to reversible *trans-cis* isomerization of azobenzene moiety upon photo-irradiation. In this paper, we have systematically studied the relationship between the layered hybrid microstructures of C3F-Azo-C6H/clay and their photoreactivity for understanding the mechanism of the photo-induced morphology change. The photoreactivity was found to be very much affected by the surrounding microenvironments. As compared with it in solution, the *cis*- to *trans*- photo-isomerization in C3F-Azo-C6H/clay nano-layered film was substantially enhanced with the quantum yield exceeding unity ( $\Phi = 1.9$ ), while the *trans*- to *cis*- isomerization was rather retarded. The corresponding hydrocarbon analogue of the azobenzene surfactant (C3H-Azo-C6H) did not show such an enhancement. The enhancement was discussed in terms of cooperative effect among adjacent azobenzene moieties along with polyfluoroalkyl chains and the inorganic clay nanosheet to prevent a dissipation of the excess energy being liberated during the photo-isomerization within the nano-layered microenvironment.

## Introduction

Various kinds of supra-molecular systems have been developed and their reactivity and functionality have been well studied in past several decades.<sup>1</sup> The research interest is currently advancing into the supra-molecular systems coupled with surrounding microenvironments in recent years.<sup>2, 3</sup> Many kinds of materials such as micelle, vesicle, liquid crystal, layered compounds, mesoporous materials, biomaterials like proteins and so on have been expected to be prospective candidates as microenvironments for developing sophisticated functions. Layered compound is also one of the most promising materials as microenvironments, which can provide unique two-dimensional interlayer spaces to the supra-molecular systems. So far, many kinds of layered compounds have been studied in synthesis,<sup>4-6</sup> exfoliation,<sup>7-12</sup> intercalation,<sup>13, 14</sup> electrochemical properties,<sup>15</sup> optical property,<sup>16</sup> catalysis,<sup>17</sup> photocatalysis<sup>18-20</sup> and so on. Especially, the intercalation of organic molecule into the interlayer spaces can provide various interesting functions such as fluorescence enhancement,<sup>21, 22</sup> efficient energy transfer<sup>23</sup> and electron transfer,<sup>24</sup> catalytic

reactions,<sup>14, 25, 26</sup> dye-sensitized solar cell (DSSC)<sup>27</sup> and artificial photosynthesis<sup>28</sup> and so on.

Molecular assemblies of polyfluorinated surfactants and their hybrids with layered compound and mesoporous materials have been successfully fabricated and studied as novel microenvironment for photochemical reactions in our group. The surface polyfluorinated micelles and vesicles can provide unique microenvironment for photochemical reactions owing to the high resistance to oxidation and the high solubility of gases as compared to hydrocarbons.<sup>29, 30</sup>

The hybrids with layered compound such as clay minerals (Sumecton SA: SSA), whose crystal structure is shown in Fig. 1a, can be successfully fabricated by the intercalation of polyfluorinated surfactant molecules (C<sub>n</sub>F-S).<sup>31-33</sup> These polyfluorinated molecules were found to intercalate in amounts exceeding the cation exchange capacity (CEC). Especially, C3F-S exhibited intercalation up to 4.4 eq. versus CEC as a saturated adsorption limit.<sup>31</sup> For providing some photo-responsive moiety to the hybrids, we have also fabricated the hybrids composed of polyfluoroalkyl azobenzene surfactant (C3F-Azo-C6H) and potassium hexaniobate (K<sub>4</sub>Nb<sub>6</sub>O<sub>17</sub>). Such kinds of photo-responsive layered hybrids show a high-density adsorption of C3F-Azo-C6H on the niobate nanosheets similar

to that of the SSA hybrids because of the small intermolecular interaction of polyfluoroalkyl chain.

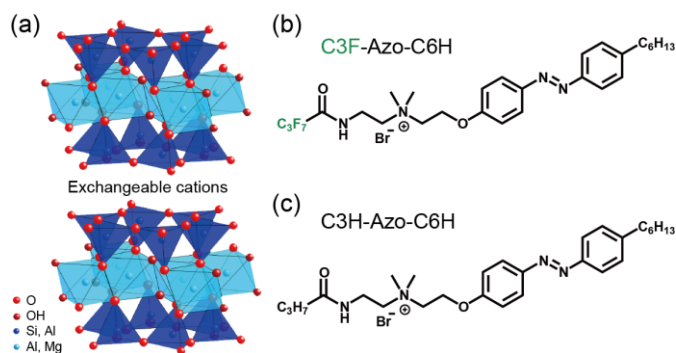


Figure 1. Crystal structure of (a) an inorganic layered clay mineral, Sumection SA and chemical structures of (b) polyfluorinated cationic surfactant (C3F-azo-C6H) and (c) alkylated cationic surfactant (C3H-azo-C6H), respectively.

Most interestingly, we have found that three-dimensional morphology changes can be induced on the hybrids by *trans-cis* photo-isomerization reaction of azobenzene group within the polyfluorinated cationic surfactants.<sup>2, 3, 34</sup> One of the highlights is a horizontal sliding of the nanosheets in a giant scale of ~1500 nm.<sup>3</sup> How can be such a giant scale change induced by a molecular shape change of ~nm scale? The system may be taken as one of artificial muscle model units. It should be, thus, most curious to clarify the molecular mechanism of the horizontal sliding of the nanosheets. Though the detailed mechanism is not fully revealed, it is convincing that the photo-isomerization reaction of C3F-Azo-C6H in the interlayer space sandwiched by nanosheets as a microenvironment is actually inducing morphology changes such as interlayer distance change and nanosheet sliding. To get a deeper insight into the morphological change in nano-layered organic/inorganic hybrid compounds, we firstly studied systematically how the photo-isomerization of azobenzene moiety within the polyfluorinated surfactant is affected by various microenvironments.

The photo-isomerization reaction of azobenzene and its derivatives have been studied by UV-Vis spectroscopy,<sup>35</sup> time-resolved transient absorption spectroscopy<sup>36, 37</sup> and time-resolved Raman spectroscopy<sup>37, 38</sup> in past several decades.

In this paper, we have investigated systematically the reactivity of molecular assembly of polyfluoroalkyl azobenzene derivative confined within the inorganic nanosheets of clay mineral in terms of its quantum yield. The molecular assemblies of C3F-Azo-C6H in the interlayer spaces of the clay hybrid showed remarkable enhancement of reactivity for *cis* to *trans* isomerization reaction upon visible light irradiation. The enhancement was discussed in terms of cooperative effect among adjacent azobenzene moieties along with polyfluoroalkyl chains and the inorganic clay nanosheet to prevent a dissipation of the excess energy being liberated during the photo-isomerization within the nano-layered microenvironment.

## Results and discussion

### Intercalation of C3F-Azo-C6H into the interlayer spaces of SSA

Nanosheets of synthetic inorganic clay, SSA, can be easily exfoliated in water and form a hybrid by intercalation of cationic molecules such as surfactant.<sup>31, 39</sup> Figure 2a shows an adsorbed amount of polyfluoroalkyl cationic surfactant having azobenzene moiety, C3F-Azo-C6H, versus CEC of SSA being dependent upon the loading level. With increasing the loading level, the adsorbed amount was increased and saturated over the loading level of 15 eq. versus CEC. In the saturated region, the adsorbed amount is 4.2 eq. versus CEC, which is in good agreement with that of C3F-S/SSA reported previously.<sup>30</sup> In the case of loading level 20 eq. versus CEC, the occupied area per one molecule adsorbed on the surface of SSA estimated by thermogravimetric analysis (TGA) was 28 Å<sup>2</sup>, which is very similar to the cross-sectional area of perfluoroalkyl chain. The occupied area (28 Å<sup>2</sup>) clearly indicates that the polyfluorinated cationic surfactant forms a bilayer structure within the interlayer space, since an occupied area for a monolayer structure should give area of twice the cross-sectional one. It is considered that C3F-Azo-C6H could high-densely adsorbed on the surface of SSA nanosheet due to the strong hydrophobicity and lipophobicity of the polyfluoroalkyl chain. XRD pattern of the C3F-Azo-C6H/SSA hybrids at each loading level is shown in Fig. 2b. With increasing the loading level, the *d*<sub>001</sub> peak gradually shifted to the smaller angle.

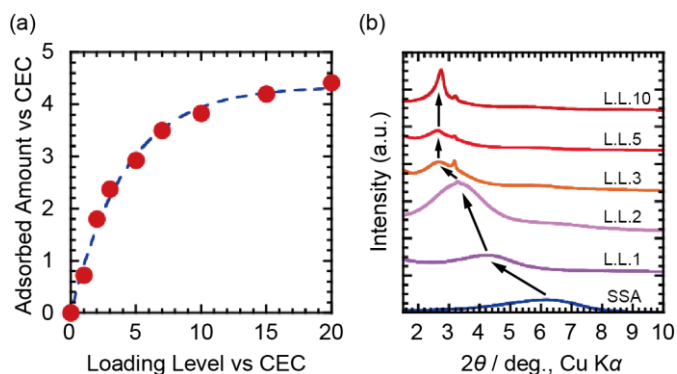


Figure 2. (a) Adsorbed amounts of C3F-Azo-C6H (versus CEC) against the loading levels (L. L.) and (b) X-ray diffraction pattern of the C3F-Azo-C6H/SSA hybrids film at each loading level.

Figure 3 shows how the basal spacing *d*<sub>001</sub> of the original SSA<sup>31</sup> change against the adsorbed amount of C3F-Azo-C6H versus CEC in the hybrids. With an increment of the adsorbed amount of C3F-Azo-C6H, the interlayer distance expanded and reached to a saturated distance, 3.4 ± 0.1 nm, at around 2.3 eq. versus CEC. The interlayer distance of the hybrid was kept constant for the further intercalation, while the adsorbed amount of C3F-Azo-C6H increased as shown in Fig. 2a. As observed in the previous C3F-S intercalation to SSA,<sup>31</sup> the C3F-Azo-C6H molecule can also induce a formation of a well-aligned structure.

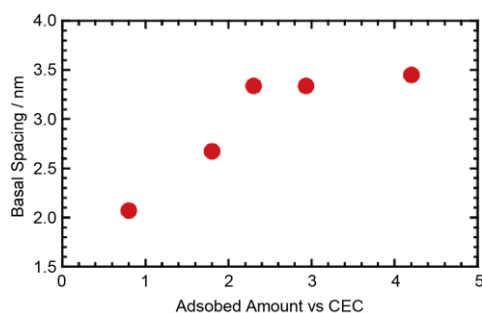


Figure 3. The basal spacing  $d_{001}$  of the hybrids against the adsorbed amount of C3F-Azo-C6H versus CEC.

The interlayer distance ( $3.4 \pm 0.1$  nm) at the saturated condition and the molecular length of C3F-Azo-C6H (3.2 nm) suggest that the C3F-Azo-C6H adsorbs with a tilting angle of  $58^\circ$  to the normal line of nanosheet surface of SSA. Since C3F-Azo-C6H forms bilayer, the tilting angle  $\theta$  is calculated by  $\cos\theta = (3.4/2)/3.2$ .

The interlayer spaces of such layered hybrids may be able to incorporate other molecules such as solvent. To check this possibility, XRD signals on the hybrid film swelled with benzene or *n*-hexane were compared with the hybrid film under the dry condition. The XRD patterns of the hybrid swelled with organic solvents are shown in Fig.S1. The hybrid film swelled with benzene showed the diffraction peak shift to the lower angle as compared to that dried in vacuum. (Fig. S1a) This indicates the interlayer distance of the hybrid expanded from 3.45 nm to 3.62 nm by the intercalation of benzene molecules. Furthermore, the XRD peak came back to the original position (3.39 nm) by drying in vacuum again. On the other hand, no diffraction peak shift was observed in the hybrid swelled with *n*-hexane (Fig. S1b), indicating that *n*-hexane molecules cannot penetrate into the interlayer spaces of the hybrid.

### Photoreaction of C3F-Azo-C6H/SSA hybrids

The spectral characteristics of C3F-Azo-C6H observed in the photo-isomerization of azobenzene moiety (Fig. 4) in various microenvironments are summarized in Table 1. The absorption peak assigned to the  $\pi$ - $\pi^*$  transition of *trans*-form of C3F-Azo-C6H is at around 344 nm, which is known to exhibit a red-shift by a J-type intermolecular interaction and a blue-shift through H-type one according to Kasha's exciton model.<sup>40</sup> It should be a good measure to observe the shift of the  $\lambda_{\max}$  for getting information on how the azobenzene moieties are mutually interacting in each microenvironment. The  $\lambda_{\max}$  of C3F-Azo-C6H in ethanol, where C3F-Azo-C6H is believed to be solubilized as a monomer molecule without mutual interaction, may be taken as the standard in judging it. All the  $\lambda_{\max}$ 's under other conditions such as, in water where a micelle is formed at the concentration ( $3.3 \times 10^{-5}$  M) examined here, in the hybrid film under the dry condition, in the hybrid film swelled with benzene, and *n*-hexane, exhibited slight red-shift, indicating mutual J-type interaction between the adjacent molecules in each microenvironment. Though it is somewhat difficult to estimate the precise spectral peak due to the light

scattering of the film sample, similarly, the isosbestic points of their spectra, where the scattering contribution is fairly small, also showed clear red shift. Since C3F-Azo-C6H is tilting against the surface of clay nanosheet, the red-shifts may be thus rationalized. On the other hand, as regards the  $\lambda_{\max}$  of *cis*-form ( $n$ - $\pi^*$  transition) showed substantial blue-shift only in water. This strongly suggests that even in micelle, water molecules penetrate into the inner core, azobenzene moieties, to form intermolecular hydrogen bonds.

Table 1. Spectral characteristics of C3F-Azo-C6H in various microenvironments.

Sample	$\lambda_{trans}$ / nm	$\lambda_{cis}$ / nm	$\lambda_{isosbestic}$ / nm
C3F-Azo-C6H in ethanol	344	440	403
C3F-Azo-C6H in water	346	434	421
Hybrid film in air	347	442	420
Hybrid film in benzene	347	441	410
Hybrid film in <i>n</i> -hexane	345	443	413

Figure 4 shows the absorption spectra of C3F-Azo-C6H/SSA hybrid film in the air upon photo-irradiation. The hybrid film had fairly good transparency probably due to the beautiful bilayer structure caused by the introduction of polyfluoroalkyl chain and the absorption spectra were measured by ordinary spectroscopic method. Upon UV light ( $\lambda = 365$ nm) irradiation, the peak at 347 nm decreased drastically. In contrast, the absorption around 442 nm, which is assigned to the  $n$ - $\pi^*$  transition of the *cis*-form of azobenzene, slightly increased and finally reached to a photo-stationary state (PSS).

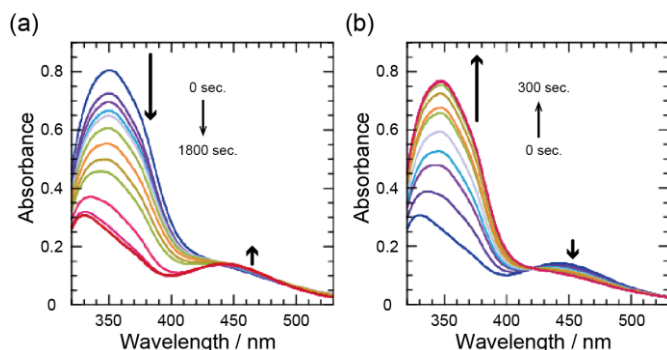


Figure 4. Absorption spectral change of C3F-Azo-C6H/SSA film (4.2 eq. vs CEC) in the air upon (a) UV and (b) visible light irradiations, respectively.

On the other hand, the photo-isomerization reaction from *cis*- to *trans*-form was efficiently induced by visible light irradiation. The hybrid film once irradiated with UV light to become rich in *cis*-form of azobenzene showed very efficient reversion to the *trans*-form upon visible light irradiation ( $\lambda = 453$  nm). To get deeper insight into what is happening within the interlayer spaces composed of polyfluoroalkyl cationic surfactant molecules and the inorganic nanosheets, a systematic

observation of the photo-isomerization of the surfactant with azobenzene group in various microenvironments was carried out. The sufficient transparency of the hybrid film enabled to estimate the photo-reactivity in terms of quantum yield. The quantum yield for photo-isomerization reaction of C3F-Azo-C6H in each microenvironment was estimated by absorption spectral change. The number of molecules converted in the reaction was calculated from the change of absorption for  $\pi$ - $\pi^*$  transition because the absorption change around 450 nm is fairly smaller as compared to that around 350 nm. Figure 5 shows the number of molecules converted for C3F-Azo-C6H/SSA film estimated from the absorption at 365 nm upon UV and visible light irradiation. At the initial stage of the photoreaction, the conversion increased drastically with gradual decrease of the slope and finally the reaction reached to the PSS. The initial slope of the time course of the reaction should correspond to the quantum yield for the photo-isomerization reaction. The internal filtering effect by the product molecules (*trans*-form) themselves should be taken into account for *cis*- to *trans*- isomerization reaction as described in experimental section. Furthermore, light scattering effect in the case of film samples for estimating the number of photons actually absorbed by azobenzene moiety also should be considered for the calculation of the quantum efficiency. (See experimental) On the basis of such careful treatment of the data, the quantum yields of the photo-isomerization for C3F-Azo-C6H in various microenvironments are summarized in Table 2. (See also Fig. S2a-g)

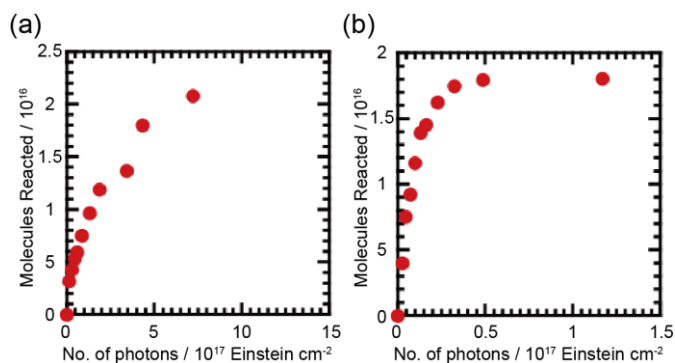


Figure 5. Molecules converted for C3F-Azo-C6H/SSA film (4.2 eq. vs CEC) estimated from the absorption at 365 nm upon UV and visible light irradiation, respectively.

Table 2. The quantum yields of photo-isomerization reaction in various microenvironments.

Sample / Microenvironment	$\Phi_{trans\ to\ cis}$	$\Phi_{cis\ to\ trans}$
C3F-Azo-C6H / Ethanol	0.35	0.64
C3F-Azo-C6H / Micelle	0.42	0.79
C3F-Azo-C6H/SSA film / Benzene	0.18	0.94
C3F-Azo-C6H/SSA film / <i>n</i> -Hexane	0.10	1.1
C3F-Azo-C6H/SSA film / Air	0.13	1.9
C3H-Azo-C6H / Ethanol	0.35	0.63
C3H-Azo-C6H / Micelle	0.36	0.77
C3H-Azo-C6H/SSA film / Air	0.09	0.42

The *trans* to *cis* isomerization reaction of C3F-Azo-C6H/SSA film was rather retarded ( $\Phi_{trans\ to\ cis} = 0.13$ ) as compared to those in ethanol ( $\Phi_{trans\ to\ cis} = 0.35$ ) and micelle (water ( $\Phi_{trans\ to\ cis} = 0.42$ )). Very interestingly, however, the *cis* to *trans* isomerization reaction of C3F-Azo-C6H/SSA in the hybrid film was remarkably enhanced compared with that in ethanol ( $\Phi_{cis\ to\ trans} = 0.64$ ) and the quantum yield exceeded unity! The quantum yield of C3F-Azo-C6H was estimated to be  $\Phi_{cis\ to\ trans} = 1.9$  in the microenvironment of hybrid film under the air atmosphere. Furthermore, the similar enhancement was observed in the C3F-Azo-C6H/SSA hybrid film moistened with benzene ( $\Phi_{cis\ to\ trans} = 0.94$ ) and *n*-hexane ( $\Phi_{cis\ to\ trans} = 1.1$ ). The hybrid moistened with *n*-hexane showed the higher reactivity than that with benzene.

On the other hand, both *trans*- to *cis*- ( $\Phi_{trans\ to\ cis} = 0.09$ ) and *cis*- to *trans*- ( $\Phi_{cis\ to\ trans} = 0.42$ ) isomerization reactions of C3H-Azo-C6H/SSA film in the air were not so efficient when compared to those of C3F-Azo-C6H. The quantum yields of azobenzene derivatives in various microenvironments were three-dimensionally shown in Fig. 6. The efficiency of the *trans*- to *cis*- isomerization reaction of C3F-Azo-C6H systematically decreased with an increase of the rigidity in the microenvironment (EtOH < Micelle < Hybrid film swelled with solvent < Hybrid film under the dry condition), while the reactivity was in the opposite order for *cis*- to *trans*- isomerization. The corresponding hydrocarbon analogue, C3H-Azo-C6H/SSA, was rather independent of the tendency. To understand the reactivity of photo-isomerization reaction, especially about the enhanced reactivity for the *cis*- to *trans*- isomerization in each microenvironment, it may be necessary to consider a possibility of contribution by a thermal process of azobenzene.

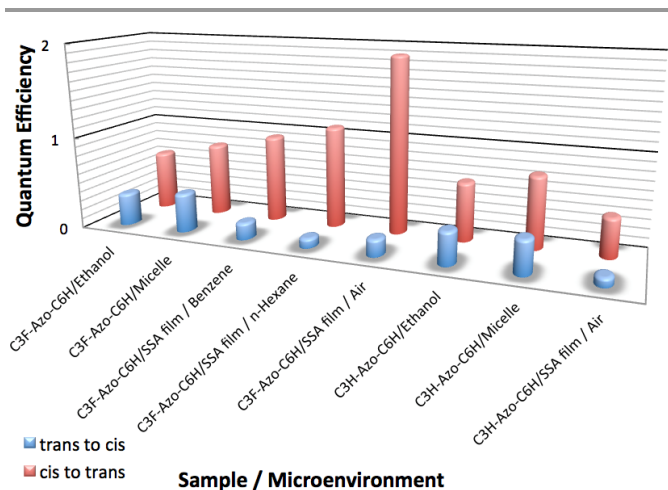


Figure 6. The quantum efficiency of cationic azobenzene surfactants and their hybrids with SSA.

### Thermal isomerization of azobenzene in the dark

The thermally induced *cis*- to *trans*- isomerization reaction of azobenzene is well known and studied by many researchers.<sup>35</sup> Figure 7a shows the time course of the absorption spectral change of C3F-Azo-C6H/SSA film at 28 °C in the dark. The absorption at 442 nm identified as a *cis*-form of C3F-Azo-C6H decreased and finally the absorption spectrum of *trans*-C3F-Azo-C6H/SSA film was obtained after 1400 sec. The rate of the reaction is analyzed in Fig. 7b. The *cis*- to *trans*-isomerization of C3F-Azo-C6H/SSA film was very slow and the pseudo-first order rate constant,  $k$ , for the thermal isomerization is estimated to be  $2.0 \times 10^{-5} \text{ s}^{-1}$  in the dark. It is thus concluded that the contribution of thermal process provided from the experimental environment (surrounding heat-bath) is negligibly small than the photochemical one, because the quantum yields of all photoreactions of C3F-Azo-C6H or C3H-Azo-C6H were measured within the initial several tens of seconds when the rate constant ( $2.0 \times 10^{-5} \text{ s}^{-1}$ ) indicates the contribution of the thermal process is negligible.

Though the thermal process induced by the surrounding heat-bath was revealed to be negligible, the C3F-Azo-C6H molecule obtains energy of 0.545 aJ and 0.452 aJ per one photon by 365 nm and 440 nm excitations, respectively. How could be the absorbed energy utilized?

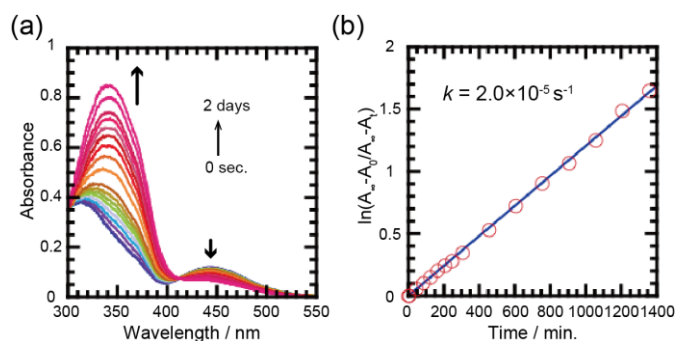


Figure 7. Thermal reactivity of C3F-AzoC6H/SSA film: (a) The absorption spectral change and (b) the rate of *cis* to *trans* isomerization reaction of C3F-Azo-C6H/SSA film (4.2 eq. vs CEC) preserved at 28 °C.

### Energy state diagram of azobenzene

Before discussing how the absorbed energy would be utilized for the isomerization reaction, it should be crucial to understand even briefly about the energy state diagram of azobenzene derivatives. According to the previous reports on azobenzene,<sup>41, 42</sup> the energy state  $S_0$  (*trans*- and *cis*-form),  $S_1$  (*trans*- and *cis*-form), and  $S_2$  (*trans*- and *cis*-form) states are depicted as Fig. 8a. The *cis*-form is destabilized by  $\sim 50 \text{ kJ mol}^{-1}$  than *trans*-form and the transition state (TS) in the ground state lies above the *cis*-form ( $S_0$ ) by  $\sim 92 \text{ kJ mol}^{-1}$ , while the potential energy surfaces in the excited states are not so straightforward. The activation energy for the thermal conversion of *cis*- into *trans*-form was reported to be  $\sim 92 \text{ kJ mol}^{-1}$  for azobenzene and here we also studied the activation energy for the conversion of *cis*- into *trans*-form for C3F-Azo-C6H in various microenvironments. (Figure S2a-q) As summarized in Table 3, the activation energy for C3F-Azo-C6H in ethanol ( $111 \text{ kJ mol}^{-1}$ ) was a little larger with azobenzene itself ( $92 \text{ kJ mol}^{-1}$ ), while in other microenvironments such as micelle ( $99 \text{ kJ mol}^{-1}$ ), C3F-Azo-C6H /clay dispersed in benzene ( $102 \text{ kJ mol}^{-1}$ ), and C3F-Azo-C6H /clay film ( $98 \text{ kJ mol}^{-1}$ ) the activation energy for the conversion from *cis*- into *trans*-form decreased in every case as compared with in ethanol. These are very suggestive that *cis*-form with increased free volume is more destabilized in more rigidly packed microenvironment such as micelle and hybrid interlayers. Level-crossing between the two parabolas of the ground state potential energy of *trans*-form and *cis*-form as depicted in Fig. 8b could explain how the activation energy would change upon the further destabilization of *cis*-form with increased free volume in the more rigid microenvironment. The actually observed decrease of the activation energy suggests the further destabilization of *cis*-form and also suggest that the structure of TS is becoming closer to *cis*-form, since the crossing point moves toward *cis*-form. The situation would lead to a presumption that upon excitation of molecule to the excited state either of  $S_1$  (*trans*- or *cis*-) or  $S_2$  (*trans*- or *cis*-), relaxation down to the ground state potential energy surface may preferably afford *trans*-form, depending on level-crossing of potential energy surfaces within the excited states and with those of the ground states. The presumption well explains the systematic enhancement of *cis*- to *trans*- isomerization in micelle and hybrid nano-layers. The remarkable enhancement of the quantum yield exceeding unity, however, still needs further explanation. Even when the enhancement is induced by the further destabilization of *cis*-form in rigid microenvironment, the maximum limit of the quantum yield should be smaller than unity! Some other factor such as a cooperating effect among the adjacent molecules should be operative in the hybrid nano-layered microenvironment in addition to the above mentioned effect on the potential energy surfaces. Further consideration can be made as follows on this point.

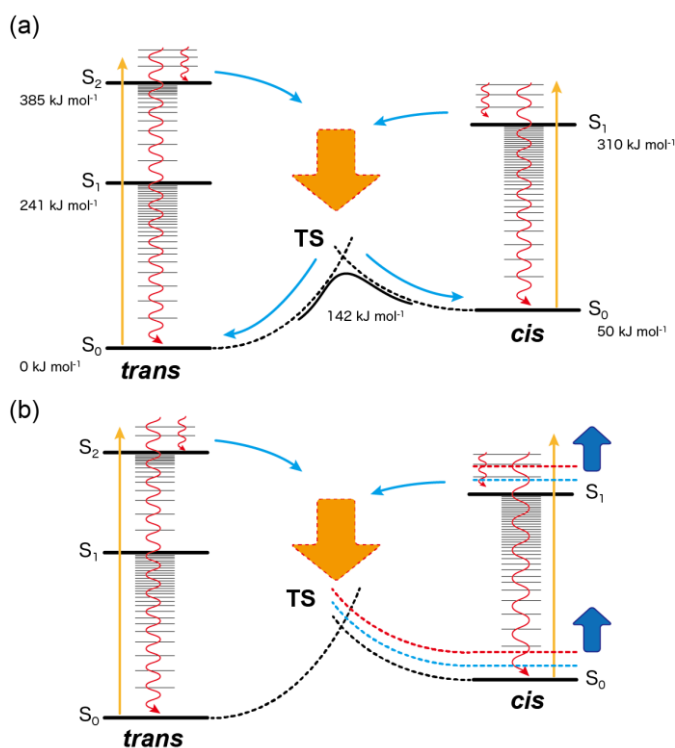


Figure 8. Schematic illustration of energy state diagrams for photo-isomerization (a) unsubstituted azobenzene and (b) C3F-Azo-C6H in microenvironment.

Table 3. The activation energy of *cis* to *trans* isomerization of C3F-Azo-C6H in various microenvironments

Sample / Microenvironment	Activation Energy / kJ mol <sup>-1</sup>
C3F-Azo-C6H / Ethanol	111
C3F-Azo-C6H / Micelle	99
C3F-Azo-C6H/SSA film / Benzene	102
C3F-Azo-C6H/SSA film / Air	98

After the photo-excitation, the excited molecule in the Franck-Condon state either in  $S_2$  ( $\pi$ - $\pi^*$ ) or  $S_1$  ( $n$ - $\pi^*$ ) would relax to the lowest vibrational level of the excited states with liberation of excess vibrational energy and suffers the reaction into the *cis*- or *trans*-form also with liberation of excess energy. In general, the most of the excess energy liberated upon vibrational relaxation or on the reaction pathway is immediately dissipated through intramolecular vibrational modes and equilibrated among them within the corresponding molecule. And subsequently the equilibrated excess energy is further dissipated to the surrounding media such as solvent molecules through V-V and V-T processes.<sup>43, 44</sup> In fluid solution such as ethanol, all the dissipation processes should be completed within ca. ten pico seconds time scale and the photochemically excited molecule is rapidly quenched to be thermally equilibrated with the surrounding solvent molecules as the external heat-bath. The negligible thermal process of isomerization induced by the external heat-bath of fluid

microenvironment as mentioned above (Figure 7) indicates that the photo-isomerization in other microenvironment than in ethanol should have the similar reactivity with it in ethanol, if the excess energy dissipation has the similar situation with it in fluid ethanol. The actual reactivities in the hybrid nano-layered environments, however, are very much different and remarkably enhanced ( $\Phi_{cis\ to\ trans} = 1.9$ ). (Table 2) These results strongly suggest that the situation of the energy dissipation is much different in the hybrid environment than that in ethanol.

In ethanol, the excess energy in the form of vibrational energy of C3F-Azo-C6H can be easily transferred to the surrounding solvent molecules and dissipates very efficiently through the microenvironments. However, in solid state such as the hybrid nano-layered microenvironment, the excess energy may be difficult to dissipate as compared to that in solution. The low efficiency of *trans*- to *cis*- isomerization in the hybrid film also implies that a local heating around the molecule caused by the retarded dissipation of excess energy prefers more population on *trans*-form by a locally heated thermal process. Very interestingly, the enhancement of *cis*- to *trans*- isomerization was not observed in the corresponding hydrocarbon analogue, C3H-Azo-C6H/SSA film. The perfluoroalkyl chain thus should play a key role in the mechanism. The weak intermolecular interaction of perfluoroalkyl chain and the well-aligned bilayer structure within the interlayer spaces may cause the retardation of the heat energy dissipation to the surrounding environment. In this viewpoint, the order of the enhancement between the hybrid dry film ( $\Phi_{cis\ to\ trans} = 1.9$ ) > the film moistened with *n*-hexane ( $\Phi_{cis\ to\ trans} = 1.1$ ) > moistened with benzene ( $\Phi_{cis\ to\ trans} = 0.94$ ) >> in ethanol ( $\Phi_{cis\ to\ trans} = 0.64$ ) well rationalize the presumption. The hybrid film moistened with benzene exhibits an expansion of the interlayer distance to allow a penetration of benzene molecule into the interlayer, while *n*-hexane does not penetrate into the interlayer as demonstrated in Figure S1. The intercalated benzene molecules would partly accept the excess energy like solvent molecules. From the viewpoint of the morphology change of the layered hybrids, such specific bilayer nanostructure, which could induce the local heating, may serve as microenvironment to induce the large reversible morphology change. Laser flash photolysis study and microscopic temperature sensing experiments are now in progress to get direct evidences of the local heating in the nano-layered microenvironment.

## Experimental

### Materials

Polyfluorinated cationic azobenzene surfactant molecule (C3F-Azo-C6H) and corresponding hydrocarbon analogue (C3H-Azo-C6H), whose chemical structures are shown in Fig. 1b and 1c, were originally synthesized in our group.<sup>2, 3</sup> Sumecton SA (SSA), which is a synthetic layered silicate with a saponite structure, was obtained from Kunimine Industries Co. Ltd. and used as a host material without further purification.

Benzene (Spectroscopic grade, Kanto Chemical Co. Ltd.), *n*-hexane (Spectroscopic grade, Kanto Chemical Co. Ltd.) and ethanol (99%, Shinwa Alcohol Industry Co., Ltd.) were used as solvents for swelling experiments. Ion-exchanged water (specific resistance:  $< 0.1 \mu\text{S cm}^{-1}$ ) was used for micelle formation.

### Sample preparation and characterization

SSA (300 mg) was dispersed in 300 mL of ion-exchanged water and used as a stock dispersion for the preparation of hybrids. Aliquot of C3F-Azo-C6H aqueous solution for each loading level (1, 2, 3, 5, 7, 10, 15 eq.) versus cation exchange capacity (CEC) was added to 10 mL of SSA dispersions and stirred at 70 °C for 5 hours. The mixture was washed with ion-exchanged water and filtrated by a hydrophilic polytetrafluoroethylene (PTFE) membrane (pore size of 0.1  $\mu\text{m}$ , Advantec). After the filtration, the resulting hybrid was dried in vacuum and stored in the dark place. The dried hybrids were analyzed by thermogravimetric/differential analysis (DTG-60H, Shimadzu), X-ray diffraction measurement (XRD, TINT-TTR III, Rigaku) and UV-Vis absorption spectroscopy (UV-2550, Shimadzu). For the preparation of the hybrid film, the appropriate amount of hybrid dispersed in *n*-hexane was cast on the cover glass. The sample film was heated at 50 °C for 3 hours in the dark before the experiment to assure the azobenzene moiety being in all *trans*-form. The sample film was also moistened with benzene or *n*-hexane for providing solvent-swelled microenvironment after inserting the film to the quartz cell (optical length: 1cm).

### Photoreaction of azobenzene

All the photo-irradiation experiments were carried out with Xenon short arc lamp (500W, USHIO) as the light source combining with an IR filter (IR cutoff filter, Edmond Optics) and band pass filters (MZ0365, ASAHI SPECTRA for 365 nm and MZ0440, ASAHI SPECTRA for 440 nm irradiation). UV (365nm, 0.18  $\text{mW cm}^{-2}$ ) or visible light (440nm, 6.5  $\text{mW cm}^{-2}$ ) irradiation of the sample solution or hybrid films was carried out for *trans*- to *cis*- and *cis*- to *trans*- isomerization reactions of azobenzene, respectively. The photoreactions were monitored by UV-Vis spectroscopy.

The quantum yield of photo-isomerization reaction was determined by Fisher method from the initial slope of the number of molecules converted versus the number of photons adsorbed under two assumptions: (1) thermal isomerization is ignored and (2) quantum yield is constant at all wavelengths.<sup>45</sup> In addition, the internal filtering effect was taken into account for the calculation of the quantum efficiency for *cis* to *trans* isomerization reaction because the masking effect due to a mixture of both *trans* and *cis* isomers should be removed for the calculation of quantum yield. In the photoreaction of the film, the scattering contribution of the sample was subtracted with the same amount of SSA film without C3F-Azo-C6H or C3H-Azo-C6H as a baseline.

### Conclusions

We have systematically investigated the photoreactivity of cationic polyfluoroalkyl azobenzene derivative, C3F-Azo-C6H, in different microenvironments. As compared with the photo-isomerization in ethanol, the quantum yield for *trans*- to *cis*-photo-isomerization reaction of C3F-Azo-C6H was smaller in the clay-hybrid with SSA. On the other hand, the *cis*- to *trans*-isomerization reaction was remarkably enhanced and the quantum yield exceeded unity. The enhancement was partly understood by a possible change of level-crossing and energy state diagram which was evidenced by the changes of the activation energy for the conversion from *cis*- to *trans*-form in the more rigid microenvironment. The irregular enhancement on the quantum yield was only explainable by a cooperative effect among the azobenzene moieties packed in the bilayer structure of perfluoroalkylated surfactants sandwiched by clay nanosheets. A presumption was postulated that a local heating around the molecule is induced by a retardation of dissipation of excess energy liberated through relaxation processes from the excited states as well as on the isomerization reaction pathway and the *trans*-form was preferably populated at the locally elevated temperature. The well-aligned perfluoroalkylated surfactants may provide the microenvironment for the retarded dissipation of the excess energy.

### Acknowledgements

This work was partially supported by a Grant-in-Aid for Young Scientists (B) from the Ministry of Education, Culture, Sports, Science and Technology of Japan.

### Notes and references

<sup>a</sup> Department of Applied Chemistry, Tokyo Metropolitan University, 1-1 Minami-osawa, Hachioji, 192-0397, Japan.

E-mail: \*inoue-haruo@tmu.ac.jp

<sup>b</sup> Center for artificial photosynthesis, Tokyo Metropolitan University, 1-1 Minami-osawa, Hachioji, 192-0397, Japan.

Electronic Supplementary Information (ESI) available:

Figure S1: XRD chart for C3F-Azo-C6H/Clay swelled with solvents.

Figure S2a-g: Quantum yield measurement data.

Figure S3a-q: Activation energy determination.

See DOI: 10.1039/b000000x/

1. J.-M. Lehn, *Supramolecular Chemistry*, VCH, Weinheim, 1995.
2. Y. Nabetani, H. Takamura, Y. Hayasaka, S. Sasamoto, Y. Tanamura, T. Shimada, D. Masui, S. Takagi, H. Tachibana, Z. Tong and H. Inoue, *Nanoscale*, 2013, **5**, 3182-3193.
3. Y. Nabetani, H. Takamura, Y. Hayasaka, T. Shimada, S. Takagi, H. Tachibana, D. Masui, Z. Tong and H. Inoue, *Journal of the American Chemical Society*, 2011, **133**, 17130-17133.
4. K. Nassau, J. W. Shiever and J. L. Bernstein, *Journal of The Electrochemical Society*, 1969, **116**, 348-353.
5. A. D. Handoko and G. K. L. Goh, *Green Chemistry*, 2010, **12**, 680-687.

6. X. Han, Q. Kuang, M. Jin, Z. Xie and L. Zheng, *Journal of the American Chemical Society*, 2009, **131**, 3152-3153.
7. T. Sasaki and M. Watanabe, *Journal of the American Chemical Society*, 1998, **120**, 4682-4689.
8. G. B. Saupe, C. C. Waraksa, H.-N. Kim, Y. J. Han, D. M. Kaschak, D. M. Skinner and T. E. Mallouk, *Chemistry of Materials*, 2000, **12**, 1556-1562.
9. R. E. Schaak and T. E. Mallouk, *Chemistry of Materials*, 2000, **12**, 3427-3434.
10. N. Miyamoto, K. Kuroda and M. Ogawa, *Journal of Materials Chemistry*, 2004, **14**, 165-170.
11. F. Geng, R. Ma, Y. Ebina, Y. Yamauchi, N. Miyamoto and T. Sasaki, *Journal of the American Chemical Society*, 2014, **136**, 5491-5500.
12. J. N. Coleman, M. Lotya, A. O'Neill, S. D. Bergin, P. J. King, U. Khan, K. Young, A. Gaucher, S. De, R. J. Smith, I. V. Shvets, S. K. Arora, G. Stanton, H.-Y. Kim, K. Lee, G. T. Kim, G. S. Duesberg, T. Hallam, J. J. Boland, J. J. Wang, J. F. Donegan, J. C. Grunlan, G. Moriarty, A. Shmeliov, R. J. Nicholls, J. M. Perkins, E. M. Grievson, K. Theuwissen, D. W. McComb, P. D. Nellist and V. Nicolosi, *Science*, 2011, **331**, 568-571.
13. T. Nakato, K. Kuroda and C. Kato, *Chemistry of Materials*, 1992, **4**, 128-132.
14. M. Ogawa and K. Kuroda, *Chemical Reviews*, 1995, **95**, 399-438.
15. N. Sakai, Y. Ebina, K. Takada and T. Sasaki, *Journal of the American Chemical Society*, 2004, **126**, 5851-5858.
16. T. Sasaki and M. Watanabe, *The Journal of Physical Chemistry B*, 1997, **101**, 10159-10161.
17. G. Centi and S. Perathoner, *Microporous and Mesoporous Materials*, 2008, **107**, 3-15.
18. J. Yu, L. Qi and M. Jaroniec, *The Journal of Physical Chemistry C*, 2010, **114**, 13118-13125.
19. Y. Miseki, H. Kato and A. Kudo, *Energy & Environmental Science*, 2009, **2**, 306-314.
20. A. Kudo and Y. Miseki, *Chemical Society Reviews*, 2009, **38**, 253-278.
21. T. Tsukamoto, T. Shimada and S. Takagi, *The Journal of Physical Chemistry A*, 2013, **117**, 7823-7832.
22. Y. Ishida, T. Shimada, H. Tachibana, H. Inoue and S. Takagi, *The Journal of Physical Chemistry A*, 2012, **116**, 12065-12072.
23. Y. Ishida, T. Shimada, D. Masui, H. Tachibana, H. Inoue and S. Takagi, *Journal of the American Chemical Society*, 2011, **133**, 14280-14286.
24. T. Yui, Y. Kobayashi, Y. Yamada, T. Tsuchino, K. Yano, T. Kajino, Y. Fukushima, T. Torimoto, H. Inoue and K. Takagi, *Physical Chemistry Chemical Physics*, 2006, **8**, 4585-4590.
25. K. Maeda, M. Eguchi, S.-H. A. Lee, W. J. Youngblood, H. Hata and T. E. Mallouk, *The Journal of Physical Chemistry C*, 2009, **113**, 7962-7969.
26. W. J. Youngblood, S.-H. A. Lee, K. Maeda and T. E. Mallouk, *Accounts of Chemical Research*, 2009, **42**, 1966-1973.
27. P. Sun, X. Zhang, X. Liu, L. Wang, C. Wang, J. Yang and Y. Liu, *Journal of Materials Chemistry*, 2012, **22**, 6389-6393.
28. K. Maeda, M. Eguchi, W. J. Youngblood and T. E. Mallouk, *Chemistry of Materials*, 2008, **20**, 6770-6778.
29. Y. Kameo, S. Takahashi, M. Krieg-Kowald, T. Ohmachi, S. Takagi and H. Inoue, *The Journal of Physical Chemistry B*, 1999, **103**, 9562-9568.
30. H. Kusaka, M. Uno, M. Krieg-Kowald, T. Ohmachi, S. Kidokoro, T. Yui, S. Takagi and H. Inoue, *Physical Chemistry Chemical Physics*, 1999, **1**, 3135-3140.
31. T. Yui, H. Yoshida, H. Tachibana, D. A. Tryk and H. Inoue, *Langmuir*, 2002, **18**, 891-896.
32. T. Yui, S. R. Uppili, T. Shimada, D. A. Tryk, H. Yoshida and H. Inoue, *Langmuir*, 2002, **18**, 4232-4239.
33. T. Yui, S. Fujii, K. Matsubara, R. Sasai, H. Tachibana, H. Yoshida, K. Takagi and H. Inoue, *Langmuir*, 2013, **29**, 10705-10712.
34. Z. Tong, S. Takagi, T. Shimada, H. Tachibana and H. Inoue, *Journal of the American Chemical Society*, 2006, **128**, 684-685.
35. H. M. D. Bandara and S. C. Burdette, *Chemical Society Reviews*, 2012, **41**, 1809-1825.
36. N. Tamai and H. Miyasaka, *Chemical Reviews*, 2000, **100**, 1875-1890.
37. T. Fujino, S. Y. Arzhantsev and T. Tahara, *Bulletin of the Chemical Society of Japan*, 2002, **75**, 1031-1040.
38. T. Fujino and T. Tahara, *The Journal of Physical Chemistry A*, 2000, **104**, 4203-4210.
39. S. Takagi, M. Eguchi, D. A. Tryk and H. Inoue, *Journal of Photochemistry and Photobiology C: Photochemistry Reviews*, 2006, **7**, 104-126.
40. M. Kasha, H. R. Rawls and M. Ashraf El-Bayoumi, in *Pure and Applied Chemistry*, 1965, vol. 11, p. 371.
41. I. K. Lednev, T.-Q. Ye, L. C. Abbott, R. E. Hester and J. N. Moore, *The Journal of Physical Chemistry A*, 1998, **102**, 9161-9166.
42. T. Schultz, J. Quenneville, B. Levine, A. Toniolo, T. J. Martinez, S. Lochbrunner, M. Schmitt, J. P. Shaffer, M. Z. Zgierski and A. Stolow, *Journal of the American Chemical Society*, 2003, **125**, 8098-8099.
43. J. B. Birks, *Photophysics of Aromatic Molecules*, John Wiley & Sons, Ltd., New York, 1970, pp. 110-112.
44. N. J. Turro, V. Ramamurthy, J. C. Scaiano, *Principles of Molecular Photochemistry An Introduction*, University Science Book, California, 2009, pp. 265-317.
45. E. Fischer, *J. Phys. Chem.*, 1967, **71**, 3704-3706.